

# ON NUMERICAL RECONSTRUCTION OF A FUNCTION FROM INCOMPLETE DATA OF ARC MEANS IN SEISMIC TOMOGRAPHY

Aleksander Denisiuk

*University of Warmia and Mazury in Olsztyn*

July 9, 2012

**Abstract.** Consider the problem of reconstruction of a small perturbation of the acoustic wave speed field from travelttime data with linear background slowness. Mathematically, the problem is equivalent to reconstruction of a function from the data of integrals along the circle arcs. The data are limited, in the sense that the arc base points belong to a compact set. We propose and numerically test a new approach, based on reduction of the problem to the inverse problem for the Radon transform. The data completion procedure is considered as well.

**Key words:** Radon transform, Seismic tomography, Inverse kinematic problem, Spherical mean transform, Interpolation of band-limited function

## 1. Introduction

Let  $H$  be a half-disk  $\{x_1^2 + x_2^2 < 1, x_2 > 0\}$ . For a function  $f$ ,  $\text{supp } f \subset H$  define the arc mean transform as an integral over an arc  $A_{a,R}$ , centered at the *daylight surface*  $\{x_2 = 0\}$ :

$$Mf(a, R) = R \int_0^\pi f(a + R \cos \varphi, R \sin \varphi) d\varphi, \quad (1)$$

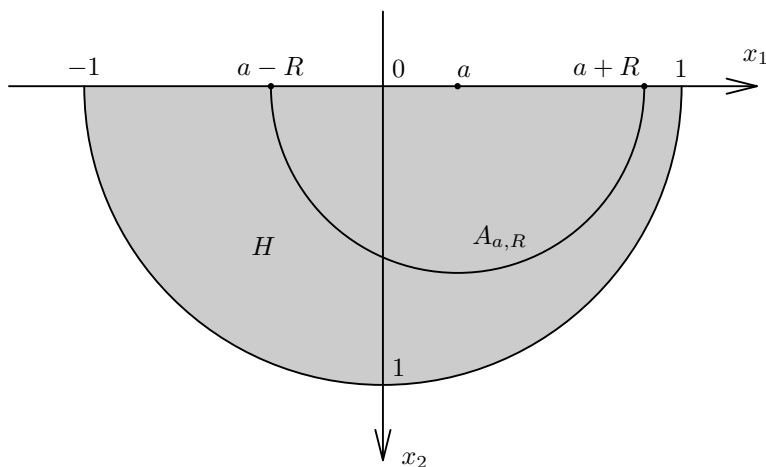
where  $a$  is the center,  $R$  is the radius of the arc, Fig. 1.

This transform appears in several applications. In seismic tomography, the travelttime in ray approximation is given by an integral:

$$T_{\text{obs}} = \int_{\text{ray}} \frac{ds}{v},$$

where  $v = v(x)$  is the velocity structure of the Earth, integration is over the ray, which is a geodesic line of the metrics  $\frac{ds}{v}$ . Under assumption that the slowness (inverse to the velocity) field of the media is of form  $1/v(x_1, x_2) = (bx_2 + c)^{-1} + \varepsilon f(x_1, x_2)$ , where  $b, c > 0$ ,  $\varepsilon \ll 1$ , the mean transform  $Mf$  in (1) is a linearized perturbation of the travel time data. We refer to books [4, 19] for the practical problem of seismic waves modeling and substantiation of this model.

In the synthetic radar aperture image processing  $f(x_1, x_2)$  is considered as a ground reflectivity and measured  $Mf(a, R)$  is interpreted as a mean reflectivity at distance  $a$  around the position of the radar carrier at a time  $R$  ([2], [8]).

Fig. 1. Domain  $H$  and arc  $A_{a,R}$ 

In thermoacoustic and photoacoustic tomography ([20, 21])  $f(x_1, x_2)$  describes the energy distribution function, and, in case of the constant wave speed, the inverse problem can be reduced to inversion of the mean operator (1).

The inversion problem for the *complete* data of arcs was considered by various authors in [4, 1, 9, 7, 6, 11, 8, 20] and some others.

We assume, that the data are known only for  $|a| + R < 1$ , i. e.  $A_{a,R} \subset H$ . Following the paper [17], we call it *the local arc problem*. The local arc problem looks more realistic from the practical point of view, at least for the seismic tomography.

In [17] the problem was reduced to the limited angle problem for the Radon transform on the plane. In [14] the problem was reduced to other incomplete data problem for the Radon transform on the plane. In [13] an algebraic discretization method based on the microlocal analysis of the geometry of the arc family was proposed. This method was implemented in [16].

In this paper we propose and numerically test a new approach, based on reduction of the problem to the inverse problem for the Radon transform. This approach is similar to considerations from [14].

In comparison with commonly-used algebraic discretization algorithms, the proposed approach gives more quick algorithm. Besides, since the problem is reduced to the standard tomographical algorithms, it is possible to apply analysis of tomographical reconstruction algorithms to the spherical mean transform.

It is well-known (cf. [18]) that the limited angle problem for the Radon transform, and therefore, the local arc problem, are ill-posed and the standard reconstruction al-

gorithms work poor. To recover as much information as possible, we propose a data completion procedure. The data completion procedure is based on the interpolation formula from [10]. As it is shown in numerical simulation, data completion permits to eliminate some artifacts in reconstruction.

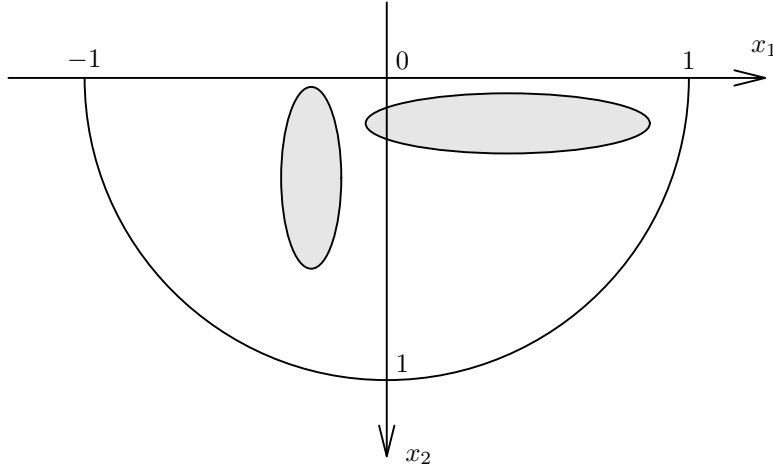


Fig. 2. Phantom function is equal to 1 inside ellipses and to 0 elsewhere

For the purpose of numerical simulation we consider a phantom, that consists of characteristic function of two ellipses with semi-axes parallel to coordinate axes (see Fig. 2). One of them is the *long* ellipse with the center at  $(-0.25, 0.33)$  and semi-axes of 0.1 and 0.3 respectively. The second is the *wide* ellipse with the center at  $(0.4, 0.15)$  and semi-axes of 0.47 and 0.1. Both ellipses locate inside the circle  $\{|x| < 0.9\}$

We will reconstruct from a discrete set of data. Fix  $N + 1 = 129$  points on the daylight surface:

$$a_k = -1 + 2k/N, \quad k = 0, \dots, N. \quad (2)$$

Denote by  $A_{k,l}$  the arc with the diameter  $[a_k, a_l]$ .

We suppose that the array  $G_{k,l}$ ,  $0 \leq k < l \leq N$  of data is known. Here  $G_{k,l}$  is the mean transform (1) for  $A_{k,l}$ .

The microlocal analysis, realized in [17], implies that reconstruction in the local arc problem is stable only in directions that are orthogonal to known arcs. In other directions the problem is of exponential instability with respect to the noise gain. Specifically, one can expect strong artifacts in form of arcs, tangent to each ellipse's boundary at point that is not covered by the given arcs.

Similarly, we expect that the boundary of wide ellipse will be reconstructed better than that of the long one. For most of the wide ellipse boundary points there is an arc

from incomplete family that is tangent to the boundary at this point. It means that most of the wide ellipse conormal bundle is covered by the family of arcs. This condition fails for most of the long ellipse boundary points. We expect only the points that are near to the daylight surface  $\{x_2 = 0\}$  will be reconstructed well. By the same reason we expect that the right side of the wide ellipse boundary and the left side of the long ellipse boundary will be reconstructed worse than opposite ones.

Despite of strong ill-posedness, reconstruction results are still of practical use. Specifically, one can consider algorithm, which recover only a part of unknown function. Such an algorithm can be stable (cf. [15]).

We test each algorithm on noisy data as well. By noisy data we mean the arc means perturbed by uniform random number up to 10% of its length. The inversion results characterizes stability of the algorithm.

## 2. Filtered back projections

In this section we reduce the problem to various incomplete data problems for the Radon transform on the plane. All unknown data in this section will be equaled to zero. The data completion procedure will be considered in section 5.

### 2.1. Limited-angle problem

The problem of reconstruction of a function by limited data of arc integrals is equivalent to the limited angle problem for the Radon transform. For  $0 < e < 1$  let  $H_e \subset H$  be a half-disk  $H_e = \{x_1^2 + x_2^2 < e^2, x_2 > 0\}$ . Let  $P_e \subset \mathbb{R}^2$  be a domain bounded by the branch of hyperbola

$$\{y_2^2 - y_1^2 = 1, y_2 > 0\} \quad (3)$$

and the line  $\{y_2 = (1 + e^2)/(1 - e^2)\}$ . (See figure 3.)

Let us rewrite the theorem from [17] in the following form:

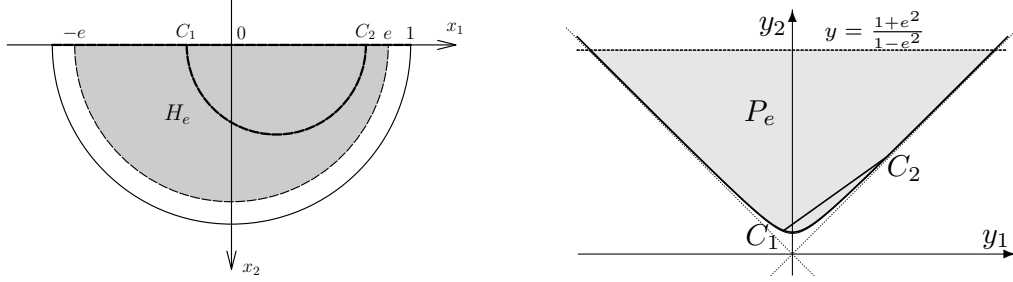
**Thrm 2.1.** Let  $f(x)$  and  $g(y)$  be two functions supported at  $H_e$  and  $P_e$  respectively. The following relations are equivalent:

$$f(x) = \frac{4x_2}{(1 - x^2)^2} g\left(\frac{2x_1}{1 - x^2}, \frac{1 + x^2}{1 - x^2}\right), \quad (4)$$

$$\mathbf{R}g(\omega, p) = \frac{1}{\sqrt{p^2 - \omega_2^2 + \omega_1^2}} \mathbf{M}f\left(-\frac{\omega_1}{p + \omega_2}, \frac{\sqrt{p^2 - \omega_2^2 + \omega_1^2}}{|p + \omega_2|}\right), \quad (5)$$

where the Radon transform is defined as follows:

$$\mathbf{R}g = \int_{\omega_1 y_1 + \omega_2 y_2 = p} g(y) ds,$$

Fig. 3. Domains  $H_e$  and  $P_e$ . Arc  $C_1C_2$  maps to line segment  $C_1C_2$ 

$ds$  is the Euclidean length element on the line  $\{\omega_1 y_1 + \omega_2 y_2 = p\}$ ,  $\omega_1^2 + \omega_2^2 = 1$ .

This theorem is based on the mapping

$$(x_1, x_2) \mapsto \left( \frac{2x_1}{1-x_2}, \frac{1+x_2}{1-x_2} \right), \quad (6)$$

which maps arcs into lines, segment  $[-1, 1] \subset \{x_2 = 0\}$  into hyperbola (3). In particular, arc  $\{|x| = e\}$  is mapped into the line  $\{y_2 = (1+e^2)/(1-e^2)\}$ . All the arcs located inside  $H$ , and, therefore intersecting the segment  $[-1, 1]$  twice, are mapped into the lines, which intersect twice the hyperbola (3).

To reconstruct the function  $f$  one should calculate the Radon transform  $Rg$  by the formula (5), then by any standard procedure recover function  $g$ , and then by (4) calculate function  $f$ .

We consider filtered backprojection algorithm for standard parallel geometry [18]. In this case one should have the values of  $Rg$  in points  $(\omega^j, s_l)$ ,  $j = 1, \dots, P$ ,  $l = -Q, \dots, Q$ , where  $\omega^j = (\cos \varphi_j, \sin \varphi_j)$ ,  $\varphi_j = \pi(j-1)/P$ ,  $s_l = l/Q$ .

To choose parameters  $P$  and  $Q$  in this algorithms, i. e. the number of angles and samples, note that  $Rg(\omega, p)$  is known only for those lines, that intersect upper branch of the hyperbola (3) in two points, i.e. for  $\pi/4 < \varphi < 3\pi/4$ . So, the known is a half of all data. The amount of given arcs is equal to  $N(N+1)/2$ . This provides the following relation:

$$P(2Q+1) = N(N+1)$$

On the other hand, the analysis realized in [18] gives the optimum relation:

$$P = \pi Q \quad (7)$$

Solving approximately this two equations, one obtains:

$$Q \approx \sqrt{N(N+1)/(2\pi)}, \quad P \approx \sqrt{\pi N(N+1)/2} \quad (8)$$

In our case ( $N = 128$ ), we get  $P = 161$ ,  $Q = 51$ .

The function to be recovered should be supported in the unit circle. So, before applying the filtered backprojection algorithm, we displace the region  $P_e$  into the unit circle with the following linear transform:

$$(y_1, y_2) \mapsto (y_1/R_e, (y_2 - C_e)/R_e), \quad (9)$$

where

$$C_e = 1/(1 - e^2) \quad (10)$$

is the “center” of  $P_e$ ,

$$R_e = \sqrt{1 + 4e^2}/(1 - e^2) \quad (11)$$

is the distance from  $C_e$  to the most far point of the boundary  $\partial P_e$  (v. picture 4). That means that instead of  $g(y)$  we consider the function  $g_1(y) = g(y_1 R_e, y_2 R_e + C_e)$ . From the properties of the Radon transform [18] we know that

$$\mathbf{R} g_1(\omega, p) = R_e^{-1} \mathbf{R} g(\omega, p R_e + C_e \omega_2).$$

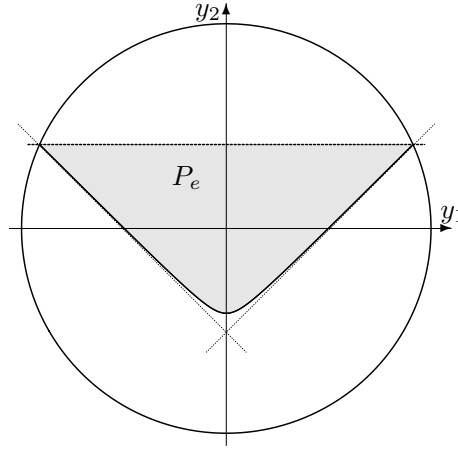


Fig. 4. Domain  $P_e$  displaced into the unit circle

The considered discrete set of arcs is not mapped into the set of parallel lines. To calculate the Radon transform with (5) we apply linear with respect to each argument

interpolation (cf. [5]). All unknown data are equaled to zero. Data completion procedure will be considered in the section 5.

Combining this considerations with filtered backprojection algorithm from [18], we obtain the following algorithm:

**Alghm 2.1.** *Step 1.* Calculate  $P$  and  $Q$  by (8),  $R_e$  by (11),  $C_e$  by (10).

*Step 2.* For  $j = 1, \dots, P$ ,  $l = -Q, \dots, Q$ , calculate interpolated Radon transform

$$R_{j,l} = \frac{N^2}{4R_e \sqrt{p^2 - \omega_2^2 + \omega_1^2}} \left( G_{k,i}(x_k - a_{k+1})(x_i - a_{i+1}) - G_{k,i+1}(x_k - a_{k+1})(x_i - a_i) \right. \\ \left. - G_{k+1,i}(x_k - a_k)(x_i - a_{i+1}) + G_{k+1,i+1}(x_k - a_k)(x_i - a_i) \right),$$

where  $\omega_1 = \cos \varphi_j$ ,  $\omega_2 = \sin \varphi_j$ ,  $\varphi_j = \pi(j-1)/P$ ,  $p = R_e l / Q + C_e \omega_2$ ,

$$x_k = -\frac{\omega_1}{p + \omega_2} - \frac{\sqrt{p^2 - \omega_2^2 + \omega_1^2}}{|p + \omega_2|}, \\ x_i = -\frac{\omega_1}{p + \omega_2} + \frac{\sqrt{p^2 - \omega_2^2 + \omega_1^2}}{|p + \omega_2|},$$

$a_k$  defined at (2). Integers  $k$  and  $i$  are chosen so that  $a_k \leq x_k < a_{k+1}$ ,  $a_i \leq x_i < a_{i+1}$ :

$$k = \left\lfloor \frac{N(x_k + 1)}{2} \right\rfloor, \quad i = \left\lfloor \frac{N(x_i + 1)}{2} \right\rfloor.$$

If  $p + \omega_2 = 0$ , the arc does not intersect  $H_e$ , so we set  $R_{i,j} = 0$ . If  $k$  or  $i$  does not belong to the segment  $[0, N]$  (data are unknown), we assume that  $G_{k,i} = 0$ .

*Step 3.* For  $j = 1, \dots, p$  calculate the convolutions

$$v_{j,k} = 1/Q \sum_{l=-Q}^Q w(k-l) R_{j,l}, \quad k = -Q, \dots, Q,$$

where  $w(l)$  is the filter. We use the Shepp-Logan filter [3]:

$$w(l) = \frac{Q^2}{\pi^2(1-4l^2)}. \quad (12)$$

*Step 4.* For each point  $x \in H_e$  calculate discrete backprojection

$$f_{FBI}(x) = \frac{4x_2}{(1-x^2)^2} \frac{2\pi}{P} \sum_{j=1}^P ((1-u)v_{j,k} + uv_{j,k+1}),$$

where  $k$  and  $u$  for each pair of  $x$  and  $j$  obtained from the following relations:

$$p = \frac{2x_1 \cos \varphi_j}{1-x^2} + \frac{(1+x^2) \sin \varphi_j}{1-x^2}, \quad k \leq Qp < k+1, \quad u = Qp - k.$$

### 3. External problem—I

The transform (6) is the composition of two mappings. One of them maps  $H$  into the unit circle and arcs centered at  $\{x_2 = 0\}$  onto straight line chords. The other is projective map, which reduces inversion problem to the limited angle problem for the Radon transform (cf. [17]). In this section we will consider only the first map:

$$(x_1, x_2) \mapsto \left( \frac{2x_1}{1+x^2}, \frac{1-x^2}{1+x^2} \right). \quad (13)$$

This map transforms  $H$  to the half-disk  $D = \{y_1^2 + y_2^2 < 1, y_2 > 0\}$  (figure 5). The diameter  $[-1, 1] \subset \{x_2 = 0\}$  of  $H$  is mapped to the upper arc  $[-1, 1] \subset \partial D$ . In this way the reconstruction problem reduces to the inversion problem for the Radon transform from the data of all lines, intersecting twice the upper arc. This is a kind of external problem for the Radon transform.

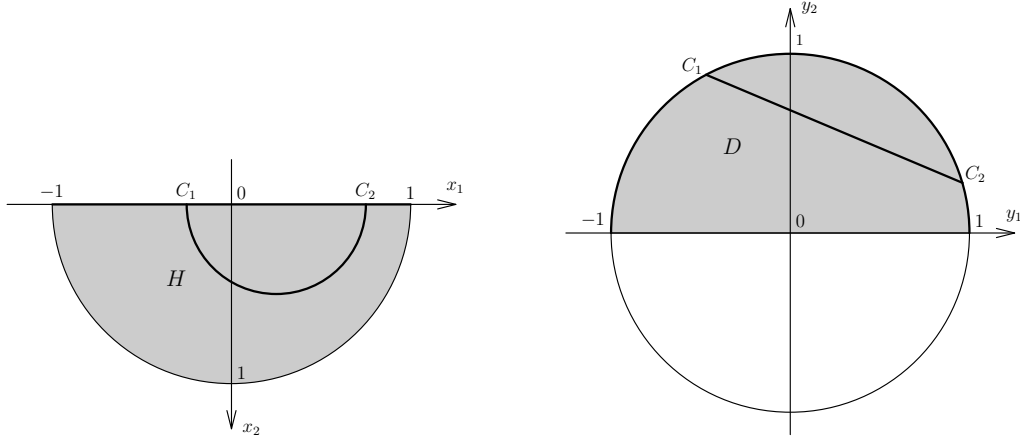


Fig. 5. Domains  $H$  and  $D$ . Arc  $C_1C_2$  maps to the line segment  $C_1C_2$

**Thrm 3.1 (cf. [14]).** Let  $f(x)$  and  $g(y)$  be two functions supported at  $H$  and  $D$  respectively. The following relations are equivalent:

$$f(x) = \frac{4x_2}{(1+x^2)^2} g\left(\frac{2x_1}{1+x^2}, \frac{1-x^2}{1+x^2}\right), \quad (14)$$

$$\mathbf{R}g(\omega, p) = \frac{1}{\sqrt{1-p^2}} \mathbf{M}f\left(\frac{\omega_1}{p+\omega_2}, \frac{\sqrt{1-p^2}}{|p+\omega_2|}\right). \quad (15)$$

Similar to the section 2.1, to reconstruct a function  $f$  one should calculate the Radon transform  $Rg$  by the formula (15), then by any standard procedure recover the function  $g$ , and then by (14) calculate  $f$ .

Again, consider the filtered backprojection algorithm for standard parallel geometry [18]. Since the support of  $g$  belongs to the unit circle, we do not need to apply any linear transform like 9.

As in the section 2.1, the discrete set of given arcs is not mapped into the set of parallel lines. To calculate the Radon transform with (15), we apply linear with respect to each argument interpolation. All the unknown data are equaled to zero. Data completion procedure will be considered in the section 5.

Parameters  $P$  and  $Q$  in parallel geometry, i.e. the number of angles and samples, can be chosen by the formulas (8).

Combining this considerations with the filtered backprojection algorithm from [18], we obtain the algorithm similar to 2.1:

**Alghm 3.1.** *Step 1.* Calculate  $P$  and  $Q$  by (8).

*Step 2.* For  $j = 1, \dots, P$ ,  $l = -Q, \dots, Q$ , calculate the interpolated Radon transform

$$R_{j,l} = \frac{N^2}{4\sqrt{1-p^2}} \left( G_{k,i}(x_k - a_{k+1})(x_i - a_{i+1}) - G_{k,i+1}(x_k - a_{k+1})(x_i - a_i) \right. \\ \left. - G_{k+1,i}(x_k - a_k)(x_l - a_{i+1}) + G_{k+1,i+1}(x_k - a_k)(x_i - a_i) \right),$$

where  $\omega_1 = \cos \varphi_j$ ,  $\omega_2 = \sin \varphi_j$ ,  $\varphi_j = \pi(j-1)/P$ ,  $p = l/Q$ ,

$$x_k = \frac{\omega_1}{p + \omega_2} - \frac{\sqrt{1-p^2}}{|p + \omega_2|}, \\ x_i = \frac{\omega_1}{p + \omega_2} + \frac{\sqrt{1-p^2}}{|p + \omega_2|},$$

$a_k$  defined at (2). Integers  $k$  and  $i$  are chosen so that  $a_k \leq x_k < a_{k+1}$ ,  $a_i \leq x_i < a_{i+1}$ :

$$k = [(x_k + 1)/(2N)], \quad i = [(x_i + 1)/(2N)].$$

If  $p + \omega_2 = 0$ , the arc does not intersect  $H$ , so we let  $R_{i,j} = 0$ . If  $k$  or  $i$  does not belong to the segment  $[0, N]$  (data are unknown), we assume that  $G_{k,i} = 0$ .

*Step 3.* For  $j = 1, \dots, p$  calculate the convolutions

$$v_{j,k} = 1/Q \sum_{l=-Q}^Q w(k-l)R_{j,l}, \quad k = -Q, \dots, Q,$$

where  $w(l)$  is the filter. We use the Shepp-Logan filter (12).

*Step 4.* For each point  $x \in H$  calculate the discrete backprojection

$$f_{FBI}(x) = \frac{4x_2}{(1+x^2)^2} \frac{2\pi}{P} \sum_{j=1}^P ((1-u)v_{j,k} + uv_{j,k+1}),$$

where  $k$  and  $u$  for each pair of  $x$  and  $j$  obtained from the following relations:

$$p = \frac{2x_2 \cos \varphi_j}{1+x^2} + \frac{(1-x^2) \sin \varphi_j}{1+x^2}, \quad k \leq Qp < k+1, \quad u = Qp - k.$$

### 3.1. External problem—II

Consider one more way of reduction of the problem to the Radon transform. Fix a point  $B = (b_1, b_2) \in H$  in which the function is to be reconstructed. Consider the following mapping:

$$(x_1, x_2) \mapsto \left( \frac{2b_2(x_1 - b_1)}{b_2^2 + (x_1 - b_1)^2 + x_2^2}, \frac{b_2^2 - (x_1 - b_1)^2 - x_2^2}{b_2^2 + (x_1 - b_1)^2 + x_2^2} \right). \quad (16)$$

The map (13) coincides with (16) for  $B = (0, 1)$ . This mapping maps  $H$  into the unit circle, arcs centered at  $\{x_2 = 0\}$  onto the chords and point  $B$  to the origin. The image of  $H$ , domain  $D_b$  is the upper part of the unit circle, bounded by the image of the boundary arc of  $H$  (figure 6). It is the chord  $C$  joining the points

$$P_+ = \left( \frac{2(1-b_1)b_2}{(1-b_1)^2 + b_2^2}, \frac{b_2^2 - (1-b_1)^2}{(1-b_1)^2 + b_2^2} \right) \text{ and } P_- = \left( \frac{-2(1+b_1)b_2}{(1+b_1)^2 + b_2^2}, \frac{b_2^2 - (1+b_1)^2}{(1+b_1)^2 + b_2^2} \right) \quad (17)$$

(the images of the points  $(\pm 1, 0)$ ). The given family of arcs (belonging to  $H$ ) transforms into the set of chords that does not intersect the chord  $C$ .

Note that when a point  $B$  tends to the daylight surface, i.e.  $b_2 \rightarrow 0$ ,  $P_{\pm} \rightarrow (-1, 0)$ . The chord  $C$  vanishes, and transformed family turned into the *complete* family of chords, contrary to the mappings (6) and (13), which provide the similar incomplete family of lines for all points  $x \in H$ .

To construct a reconstruction algorithm we have to prove an analog to the theorems 2.1, and 3.1.

**Thrm 3.2.** Let  $f(x)$  and  $g(y)$  be two functions, supported at  $H$  and  $D_b$  respectively. The following relations are equivalent:

$$f(x) = \frac{4b_2^2 x_2}{(b_2^2 + (x_1 - b_1)^2 + x_2^2)^2} g\left(\frac{2b_2(x_1 - b_1)}{b_2^2 + (x_1 - b_1)^2 + x_2^2}, \frac{b_2^2 - (x_1 - b_1)^2 - x_2^2}{b_2^2 + (x_1 - b_1)^2 + x_2^2}\right), \quad (18)$$

$$\mathbf{R}g(\omega, p) = \frac{1}{\sqrt{1-p^2}} \mathbf{M}f\left(b_1 + \frac{\omega_1 b_2}{p + \omega_2}, \frac{b_2 \sqrt{1-p^2}}{|p + \omega_2|}\right). \quad (19)$$

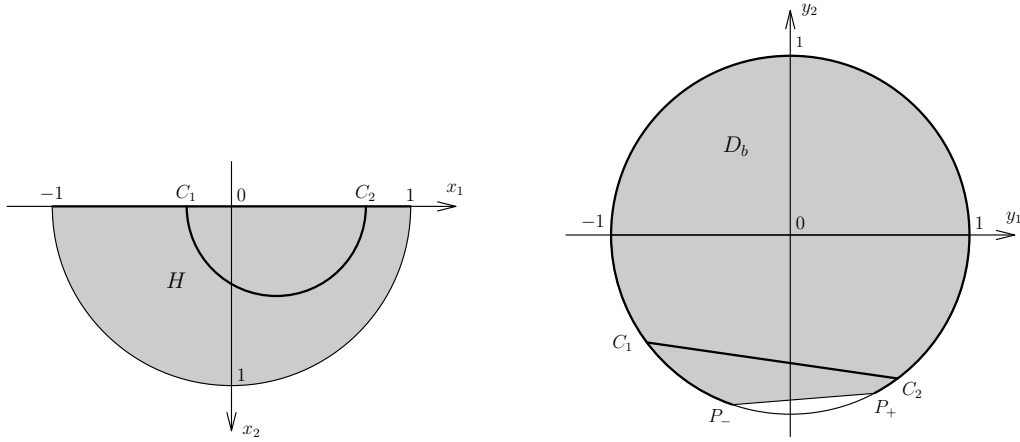


Fig. 6. Domains  $H$  and  $D_b$  ( $B = (0.2, 0.2)$ ). Arc  $C_1C_2$  maps to the line segment  $C_1C_2$

**Proof:** The proof of the theorem is a straightforward calculation (cf. [14], [17]). Consider the mapping (16), which provides diffeomorphism between  $H$  and  $D$ . Pulling the equation of the line  $\omega_1 y_1 + \omega_2 y_2 = p$  from  $D_b$  back to  $H$ , one obtains, after some simplification, the equation of the arc:

$$\left( x_1 - \left( b_1 + \frac{\omega_1 b_2}{p + \omega_2} \right) \right)^2 + x_2^2 = \frac{1 - p^2}{(p + \omega_2)^2}.$$

Let's push forward the integral (1) from  $H$  to  $D_b$ :

$$Mf(a, R) = \int_{\omega_1 y_1 + \omega_2 y_2 = p} f((x(y))) ds_H,$$

where parameters  $(\omega, p)$  and  $(a, R)$  are related as in (19),  $ds_H$  is the image of the Euclidean measure on the arc under the mapping (16). To calculate  $ds_H$  one can use its invariant definition:

$$ds_H = \frac{dy_H}{d\psi(y)} \|\text{grad } \psi\|_H|_{\psi(y)=0},$$

where  $\psi(y) = \omega_1 y_1 + \omega_2 y_2 - p$ ,  $dy_H/d\psi$  is the Leray form, i. e. the form  $\rho$  such that  $dy_H = d\psi \wedge \rho$ . Norm, gradient and the volume element  $dy_H$  are calculated with respect to the image of the Euclidean metric under (16). By direct calculation this image is equal to

$$b_2^2 \frac{(1 - y_2^2) dy_1^2 + 2y_1 y_2 dy_1 dy_2 + (1 - y_1^2) dy_2^2}{(1 + y_2)^2 (1 - y^2)}.$$

Therefore

$$dy_H = \frac{b_2^2 dy}{\sqrt{1-y^2}(1+y_2)^2},$$

$$\|\text{grad } \psi\|_H|_{\psi(y)=0} = b_2^{-2}(1+y_2)^2(1-p^2),$$

$$ds_H = \frac{dy}{d\psi} \frac{b_2 \sqrt{1-p^2}}{(1+y_2)\sqrt{1-y^2}} = \sqrt{1-p^2} \frac{((x_1-b_1)^2 + x_2^2 + b_2^2)^2}{4b_2^2 x_2} ds,$$

where  $ds = dy/d\psi(y)$  is the Euclidean measure on the line.

The theorem is proved.

So, to reconstruct  $f(b_1, b_2)$ , one should calculate the Radon transform  $Rg$  by the formula (19), then, by any standard procedure recover function  $g(0, 0)$ , and then by (18) calculate function  $f$ , substituting  $x_1 = b_1$ ,  $x_2 = b_2$ .

As usual, consider filtered backprojection algorithm for standard parallel geometry and Shepp-Logan filter (12).

To compute parameters  $P$  and  $Q$  in this algorithms, i. e. the number of angles and samples, let us estimate the portion of known data. Consider the projective transform which maps points  $P_{\pm}$  to the infinity. Apply this transform to the incomplete data reconstruction problem for the Radon transform considered in this section. The problem is reduced to the limited angle problem for the Radon transform with unknown angle range of  $\theta/2$  (cf. [12], [17]), where  $\theta$  is the angle measure of the arc  $(P_- P_+)$  of the unit circle. So we can think that the portion of known data equals  $(\pi - \theta/2)/\pi$ . This will give us the following relation:

$$P(2Q + 1) \left( \frac{\pi - \theta/2}{\pi} \right) = \frac{N(N + 1)}{2}$$

Solving approximately this equation together with optimal relation (7) one obtains the formulas:

$$Q \approx \sqrt{\frac{N(N + 1)}{2(2\pi - \theta)}} \quad P \approx \pi \sqrt{\frac{N(N + 1)}{2(2\pi - \theta)}} \quad (20)$$

Using explicit formulas for the coordinates of  $P_{\pm}$  (17) we obtain the formula for  $\theta$ :

$$\theta = \pi - \arcsin \left( \frac{(1 + b_1)^2 - b_2^2}{(1 + b_1)^2 + b_2^2} \right) - \arcsin \left( \frac{(1 - b_1)^2 - b_2^2}{(1 - b_1)^2 + b_2^2} \right) \quad (21)$$

**Alghm 3.2.** *Step 1.* Calculate  $P$  and  $Q$  by (20) and (21).

*Step 2.* For  $j = 1, \dots, P$ ,  $l = -Q, \dots, Q$ , calculate the interpolated Radon transform

$$R_{j,l} = \frac{N^2}{4\sqrt{1-p^2}} \left( G_{k,i}(x_k - a_{k+1})(x_i - a_{i+1}) - G_{k,i+1}(x_k - a_{k+1})(x_i - a_i) \right. \\ \left. - G_{k+1,i}(x_k - a_k)(x_i - a_{i+1}) + G_{k+1,i+1}(x_k - a_k)(x_i - a_i) \right), \quad (22)$$

where  $\omega_1 = \cos \varphi_j$ ,  $\omega_2 = \sin \varphi_j$ ,  $\varphi_j = \pi(j-1)/P$ ,  $p = l/Q$ ,

$$x_k = b_1 + \frac{\omega_1 b_2}{p + \omega_2} - b_2 \frac{\sqrt{1-p^2}}{|p + \omega_2|}, \quad (23)$$

$$x_i = b_1 + \frac{\omega_1 b_2}{p + \omega_2} + b_2 \frac{\sqrt{1-p^2}}{|p + \omega_2|}, \quad (24)$$

$a_k$  defined at (2). Integers  $k$  and  $i$  are chosen so that  $a_k \leq x_k < a_{k+1}$ ,  $a_i \leq x_i < a_{i+1}$ :

$$k = [(x_k + 1)/(2N)], \quad i = [(x_i + 1)/(2N)].$$

If  $p + \omega_2 = 0$ , the arc does not intersect  $H$ , so we let  $R_{i,j} = 0$ . If  $k$  or  $i$  does not belong to the segment  $[0, N]$  (data are unknown), we assume that  $G_{k,i} = 0$ .

*Step 3.* For  $j = 1, \dots, p$  calculate the convolutions

$$v_{j,0} = 1/Q \sum_{l=-Q}^Q w(-l) R_{j,l},$$

where  $w(l)$  is defined in (12).

*Step 4.* Calculate the discrete backprojection

$$f_{FBI}(b_1, b_2) = \frac{4}{b_2} \frac{2\pi}{P} \sum_{j=1}^P v_{j,0}. \quad (25)$$

### 3.2. Numerical tests

Numerical tests for algorithms 2.1, 3.1, 3.2 are presented on the figure 7. The left row presents the reconstruction after exact data, the right row—after noisy data.

The reconstruction with algorithm 2.1 (on the top) looks less detailed, but it has smaller artifacts. Furthermore, the reconstruction is more stable, there is a little difference between reconstruction by exact and noisy data. Another advantage of this method is that algorithm is far quicker than algebraic algorithms.

The second line contains reconstruction with the algorithm 3.1. It looks more detailed then reconstruction by the algorithm 2.1.

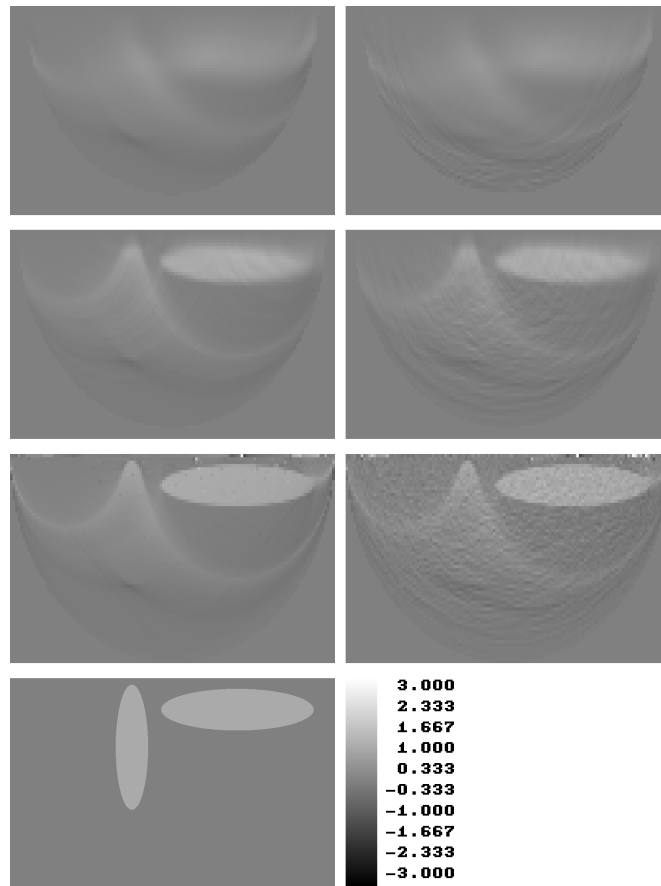


Fig. 7. Reconstruction with the filtered backprojection algorithms: 2.1, 3.1, 3.2 (from the top) for exact (left) and noisy (right) data.

The third line presents reconstruction with the algorithm 3.2. This reconstruction looks more precise and detailed than previous ones. In particular, the boundary of the wide ellipse and the upper boundary of the long ellipse look more sharp. On the other hand, the reconstruction has larger and more artifacts, and is more unstable. One of the sources of instability is the little factor  $b_2$  in denominator in (25), which increases the errors especially near the boundary. The other disadvantage of the algorithm is that all the parameter  $P$ ,  $Q$ ,  $R_{i,j}$  essentially depends on  $(b_1, b_2)$ , (see (20), (21), (22)), so one should recalculate it for all the reconstruction points. This increases the computing time.

#### 4. Local reconstruction

##### 4.1. Reconstruction in the neighborhood of a fixed point

Consider another application of the theorem 3.2. Fix a point  $B = (b_1, b_2)$ , called the *center* of the reconstruction. To reconstruct the function  $f$  one should calculate the Radon transform  $Rg$  by the formula (19), then by any standard procedure recover function  $g(y)$ , and then by (18) calculate function  $f$ . This leads us to the following algorithm.

**Alghm 4.1.** *Step 1.* Fix point  $B = (b_1, b_2)$ . Calculate  $P$  and  $Q$  by (20) and (21).

*Step 2.* For  $j = 1, \dots, P$ ,  $l = -Q, \dots, Q$ , calculate the interpolated Radon transform

$$R_{j,l} = \frac{N^2}{4\sqrt{1-p^2}} \left( G_{k,i}(x_k - a_{k+1})(x_i - a_{i+1}) - G_{k,i+1}(x_k - a_{k+1})(x_i - a_i) \right. \\ \left. - G_{k+1,i}(x_k - a_k)(x_i - a_{i+1}) + G_{k+1,i+1}(x_k - a_k)(x_i - a_i) \right), \quad (26)$$

where  $\omega_1 = \cos \varphi_j$ ,  $\omega_2 = \sin \varphi_j$ ,  $\varphi_j = \pi(j-1)/P$ ,  $p = l/Q$ ,

$$x_k = b_1 + \frac{\omega_1 b_2}{p + \omega_2} - b_2 \frac{\sqrt{1-p^2}}{|p + \omega_2|}, \\ x_i = b_1 + \frac{\omega_1 b_2}{p + \omega_2} + b_2 \frac{\sqrt{1-p^2}}{|p + \omega_2|},$$

$a_k$  defined at (2). Integers  $k$  and  $i$  are chosen so that  $a_k \leq x_k < a_{k+1}$ ,  $a_i \leq x_i < a_{i+1}$ :

$$k = [(x_k + 1)/(2N)], \quad i = [(x_i + 1)/(2N)].$$

If  $p + \omega_2 = 0$ , the arc does not intersect  $H$ , so we let  $R_{i,j} = 0$ . If  $k$  or  $i$  does not belong to the segment  $[0, N]$  (data are unknown), we assume that  $G_{k,i} = 0$ .

*Step 3.* For  $j = 1, \dots, p$  calculate the convolutions

$$v_{j,k} = 1/Q \sum_{l=-Q}^Q w(k-l)R_{j,l}, \quad k = -l, \dots, l,$$

where  $w(l)$  is the filter. We use the Shepp-Logan filter (12).

*Step 4.* For any point  $x \in H$  calculate discrete backprojection

$$f_{FBI}(x) = \frac{4b_2^2 x_2}{(b_2^2 + (x_1 - b_1)^2 + x_2^2)^2} \frac{2\pi}{P} \sum_{j=1}^P ((1-u)v_{j,k} + uv_{j,k+1}),$$

where  $k$  and  $u$  for each pair of  $x$  and  $j$  obtained from the following relations:

$$p = \frac{2b_2(x_1 - b_1) \cos \varphi_j}{b_2^2 + (x_1 - b_1)^2 + x_2^2} + \frac{(b_2^2 - (x_1 - b_1)^2 - x_2^2) \sin \varphi_j}{b_2^2 + (x_1 - b_1)^2 + x_2^2}, \quad (27)$$

$$k \leq Qp < k + 1, \quad u = Qp - k. \quad (28)$$

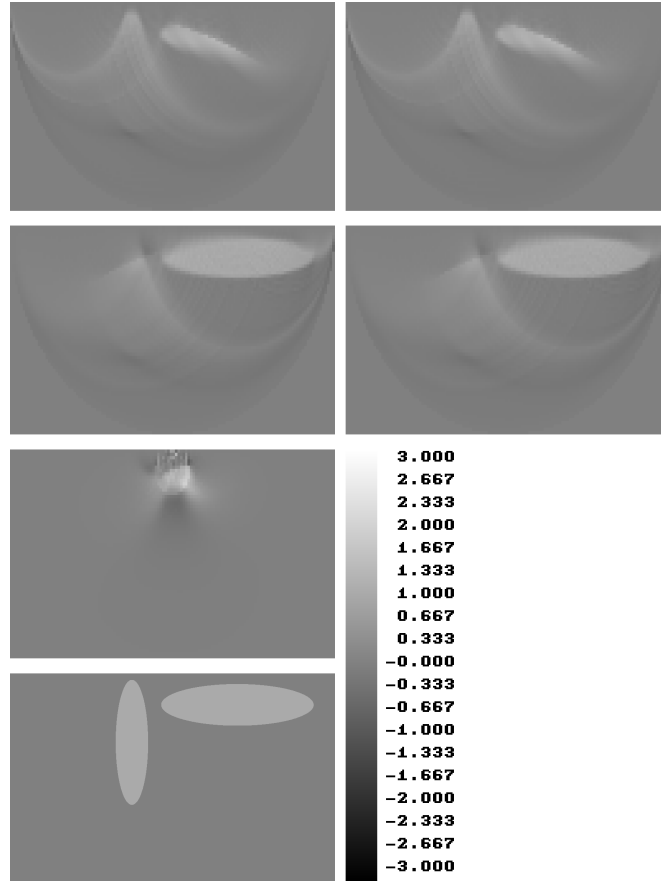


Fig. 8. Local reconstruction with the centers  $(-0.5, 0.5)$ ,  $(0.5, 0.5)$ ,  $(0, 0.025)$  (from the top) for exact (left) and noisy (right) data.

The numerical results are presented at the figure 8. We call it *the local reconstruction* since the reconstruction is good only in a neighborhood of the center  $B$ . The details

that are far from  $B$  are illegible. This method works ill, if  $b_2$  is small. Note that method looks to be stable and is as quick as algorithms 2.1 and 3.1.

#### 4.2. Combined local reconstruction

One can take the advantage of detailedness of the algorithm 3.2 and of speed of the algorithm 4.1 in the following way. Divide investigated region into several regions. For each region perform local reconstruction algorithm with the center of reconstruction located inside this region. Glue together the results of reconstruction.

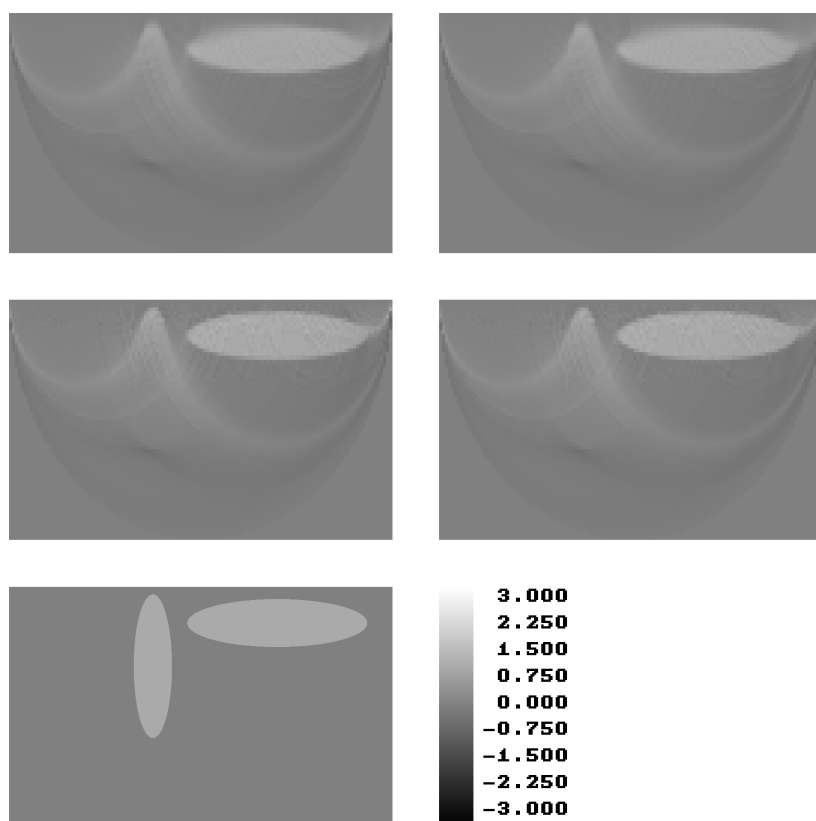


Fig. 9. Combined reconstruction for exact (left) and noisy (right) data. The region divided into two (at the top) and 18 squares.

In the figure 9 the numerical results are presented. The region is divided into 18 squares. The centers of reconstruction are the centers of the squares. One can

see that the method gives stable detailed reconstruction while computing time is smaller than in algebraic algorithms as well as in the algorithm 3.2.

## 5. Data completion

### 5.1. Interpolation procedure

In this section we consider the procedure of data completion for the local arc problem. We will make use of the theorem 2.1. Since the local arc problem is equivalent to the limited angle problem for Radon transform, consider the data completion procedure for the last problem.

Suppose that the Radon transform  $Rf(\omega, p)$  of a finite function  $f$  is unknown for  $|\omega_n| > \lambda|\omega'|$  for certain  $\lambda > 0$ , where  $\omega' = (\omega_1, \dots, \omega_{n-1})$ . Following the paper [10] we start with the relation between the Radon and Fourier transforms:

$$\tilde{f}(s \cdot \omega) = \int Rf(\omega, p) e^{-ips} dp. \quad (29)$$

Limited angle problem is equivalent to interpolation of Fourier transform of finite function  $\tilde{f}(\xi)$ , unknown in the cone  $\{|\xi_n| > \lambda|\xi'|\}$ , where  $\xi' = (\xi_1, \dots, \xi_{n-1})$ . The last problem can be solved with the explicit formula [10]:

$$\tilde{f}(\xi', \xi_n) = \frac{1}{\pi} e^{R\sqrt{\rho^2 - \xi_n^2}} \int_{|\eta| > \rho} \frac{\sin R\sqrt{\eta^2 - \rho^2}}{|\eta - \xi_n|} \tilde{f}(\xi', \eta) d\eta, \quad (30)$$

where  $\rho = \lambda|\xi'|$ ,  $\xi_n \in [-\rho, \rho]$ ,  $\text{supp } f \subset \{|x| \leq R\}$ .

To construct the numerical algorithm based on the formula (30) note that the reconstruction algorithms 2.1–4.1 include filtration. We will interpolate *filtered Radon transform*:

$$R_\Lambda f(\omega, p) = \frac{1}{2\pi} \int_{-\Lambda}^{\Lambda} \tilde{f}(s \cdot \omega) e^{isp} ds. \quad (31)$$

Substituting in (31) formulas (30) and (29) and calculating explicitly integral with respect to  $s$  one obtains the following formula (cf. [10]):

$$\begin{aligned} R_\Lambda(\omega, p) &= \frac{1}{2\pi} \int_0^\infty d\beta \int \frac{\beta E_\nu(\alpha, \beta, \gamma)}{\sqrt{\rho^2 + \beta^2}} \\ &\times \left( \frac{Rf((\omega', \sqrt{\rho^2 + \beta^2}), p - R\alpha)}{|\sqrt{\rho^2 + \beta^2} - \omega_n|} + \frac{Rf((\omega', -\sqrt{\rho^2 + \beta^2}), p - R\alpha)}{|\sqrt{\rho^2 + \beta^2} + \omega_n|} \right) d\alpha, \end{aligned} \quad (32)$$

where

$$E_\nu(\alpha, \beta, \gamma) = 2\beta \frac{\gamma^2 - \alpha^2 + \beta^2}{(\gamma^2 + (\alpha + \beta)^2)(\gamma^2 + (\alpha - \beta)^2)} + e^{\gamma\nu} \left( \frac{\gamma \sin \nu(\alpha + \beta) - (\alpha + \beta) \cos \nu(\alpha + \beta)}{\gamma^2 + (\alpha + \beta)^2} - \frac{\gamma \sin \nu(\alpha - \beta) - (\alpha - \beta) \cos \nu(\alpha - \beta)}{\gamma^2 + (\alpha - \beta)^2} \right),$$

$\gamma = \sqrt{\rho^2 - \omega_n^2}$ ,  $|\omega_n| > \lambda|\omega'|$ ,  $\rho = \lambda|\omega'|$ ,  $\nu = \Lambda R$ —the parameter which characterizes the detailedness of the reconstruction.

## 5.2. Implementation

For numerical implementation split the integral (32):

$$\mathbf{R}_\Lambda f(\omega, p) = I_{no} + I_{sp} - I_{sm} + I_{cm} - I_{cp},$$

where

$$I_{no} = \frac{1}{\pi^2} \int_0^\infty d\beta \int \frac{\beta^2(\gamma^2 - \alpha^2 + \beta^2)}{\sqrt{\rho^2 + \beta^2}(\gamma^2 + (\alpha + \beta)^2)(\gamma^2 + (\alpha - \beta)^2)} G(\alpha, \beta) d\alpha, \quad (33)$$

$$I_{sp} = \frac{\gamma e^{\nu\gamma}}{2\pi^2} \int_0^\infty d\beta \int \frac{\sin \nu(\alpha + \beta)}{\gamma^2 + (\alpha + \beta)^2} \frac{\beta}{\sqrt{\rho^2 + \beta^2}} G(\alpha, \beta) d\alpha, \quad (34)$$

$$I_{sm} = \frac{\gamma e^{\nu\gamma}}{2\pi^2} \int_0^\infty d\beta \int \frac{\sin \nu(\alpha - \beta)}{\gamma^2 + (\alpha - \beta)^2} \frac{\beta}{\sqrt{\rho^2 + \beta^2}} G(\alpha, \beta) d\alpha, \quad (35)$$

$$I_{cp} = \frac{e^{\nu\gamma}}{2\pi^2} \int_0^\infty d\beta \int \frac{\cos \nu(\alpha + \beta)}{\gamma^2 + (\alpha + \beta)^2} \frac{\beta(\alpha + \beta)}{\sqrt{\rho^2 + \beta^2}} G(\alpha, \beta) d\alpha, \quad (36)$$

$$I_{cm} = \frac{e^{\nu\gamma}}{2\pi^2} \int_0^\infty d\beta \int \frac{\cos \nu(\alpha - \beta)}{\gamma^2 + (\alpha - \beta)^2} \frac{\beta(\alpha - \beta)}{\sqrt{\rho^2 + \beta^2}} G(\alpha, \beta) d\alpha, \quad (37)$$

$$G(\alpha, \beta) = \frac{\mathbf{R}f((\omega', \sqrt{\rho^2 + \beta^2}), p - R\alpha)}{|\sqrt{\rho^2 + \beta^2} - \omega_n|} + \frac{\mathbf{R}f((\omega', -\sqrt{\rho^2 + \beta^2}), p - R\alpha)}{|\sqrt{\rho^2 + \beta^2} + \omega_n|}. \quad (38)$$

We evaluate integrals (33)–(37) as multiple iterated.

Because of finiteness of  $f$  the function  $G(\alpha, \beta)$  (38) vanishes when  $|p - R\alpha| \geq R\sqrt{|\omega'|^2 + \rho^2 + \beta^2}$ , so internal integrals in (33)–(37) are along the finite segment  $[A_-, A_+]$ ,  $A_\pm = p/R \pm \sqrt{|\omega'|^2 + \rho^2 + \beta^2}$ .

To cut integrals with respect to  $\beta$  note that in (33), (36), (37) integrands decrease as  $O(\beta^{-3})$  while in (34)–(35) as  $O(\beta^{-4})$  when  $\beta \rightarrow \infty$ . So, one can consider finite segment

respectively  $[0, \varepsilon^{-1/2}]$  or  $[0, \varepsilon^{-1/4}]$ , where  $\varepsilon$  is the desired accuracy. In numerical tests we set  $\varepsilon = 0.01$ .

To choose the filtration level  $\Lambda$ , note that there is a factor  $e^{\gamma\nu} = e^{\gamma R\Lambda}$  in the integrals (34)–(37), which increases a computational error. So  $\Lambda$  should not be very large. For instance, in our computation we set  $\Lambda = \ln(25)/(R\gamma)$ , so computation error increases  $\approx 25$  times.

The integral (33) is evaluated by the trapezoid rule with  $N - 1$  internal nodes, like integrals in standard filtered backprojection tomography algorithms (cf. [18]).

Integrals (34)–(37) we evaluate with analogous formula, considering oscillating trigonometric factors as a weight functions:

$$\int_a^b f(x) \sin \nu x \, dx \approx \frac{\sin \nu \frac{h}{2}}{\nu \frac{h}{2}} \frac{\sin \nu \frac{h}{2}}{\frac{\nu}{2}} \sum_{i=1}^{N-1} f(x_i) \sin \nu x_i$$

$$+ f(a) \left( \frac{\cos \nu a}{\nu} - \frac{\cos \nu(a + \frac{h}{2}) \sin \nu \frac{h}{2}}{\nu \frac{h}{2}} \right) + f(b) \left( -\frac{\cos \nu b}{\nu} + \frac{\cos \nu(b - \frac{h}{2}) \sin \nu \frac{h}{2}}{\nu \frac{h}{2}} \right),$$

$$\int_a^b f(x) \cos \nu x \, dx \approx \frac{\sin \nu \frac{h}{2}}{\nu \frac{h}{2}} \frac{\sin \nu \frac{h}{2}}{\frac{\nu}{2}} \sum_{i=1}^{N-1} f(x_i) \cos \nu x_i$$

$$+ f(a) \left( -\frac{\sin \nu a}{\nu} + \frac{\sin \nu(a + \frac{h}{2}) \sin \nu \frac{h}{2}}{\nu \frac{h}{2}} \right) + f(b) \left( \frac{\sin \nu b}{\nu} - \frac{\sin \nu(b - \frac{h}{2}) \sin \nu \frac{h}{2}}{\nu \frac{h}{2}} \right),$$

where  $h = (b - a)/N$ .

In numerical tests we used  $N/2 = 64$  nodes for the integrals (33)–(37) with respect to  $\alpha$  and  $N = 128$  for these integrals with respect to  $\beta$ . The common amount of the nodes  $N^2/2$  approximately coincides with  $N(N + 1)/2$ —the amount of given data.

### 5.3. Numerical tests

To perform the numerical test we add to the nodes (2) on the daylight surface new ones. As in the section 2.1, we think that the half of the data are known. So we add  $N/4 = 32$  nodes to the left from the segment  $[-1, 1]$ , and  $N/4 = 32$ —to the right:

$$\ell_j = -\tan \frac{\pi}{4} \left( 1 + \frac{4j}{N+1} \right), \quad j = 1, \dots, N/4,$$

$$r_j = \tan \frac{\pi}{4} \left( 1 + \frac{4j}{N+1} \right), \quad j = 1, \dots, N/4. \tag{39}$$

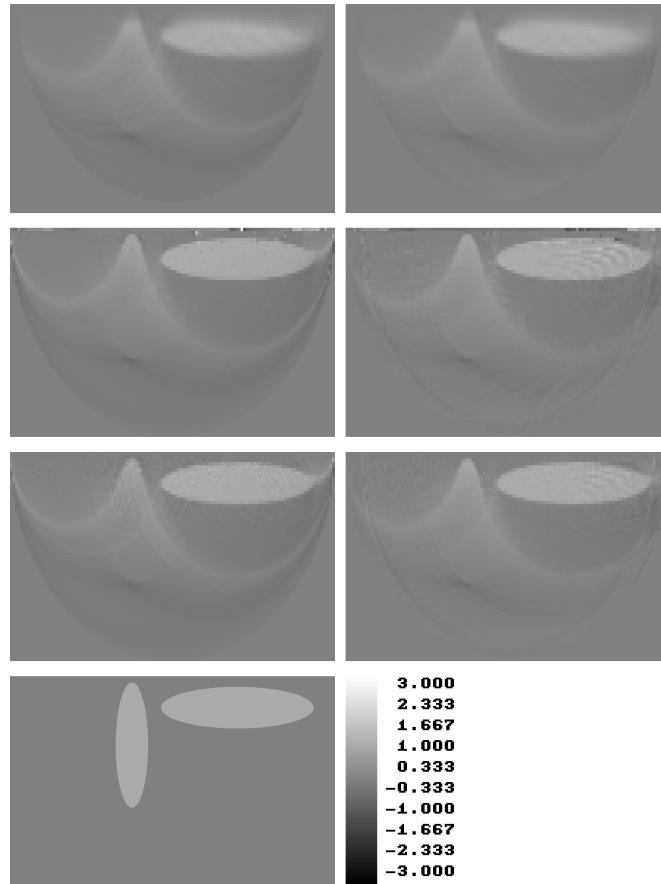


Fig. 10. Reconstruction with the interpolated (right) and given (left) data for exact data by algorithms: 3.1, 3.2, 4.1—the region is divided into 18 squares.

Note that the distance between the neighboring nodes  $\ell_j$  and  $r_j$  increases when  $j \rightarrow \infty$ , so the new family is transformed into “almost uniform” family under the map (6).

We add to the known data array  $G_{k,l}$  interpolated values of the arc mean transform for arcs gathering nodes  $\ell_j$  and  $r_j$  with given nodes  $a_k$ .

To compute the values of  $Rf(\omega, p)$  in the nodes of quadrature formulas we used linear interpolation with respect to each coordinates.

To use completed data in the algorithms 2.1, 3.1, 3.2, and 4.1 we make changes in the step 2. After calculating the feet of the arc  $x_k$  and  $x_i$  with the corresponding formula we

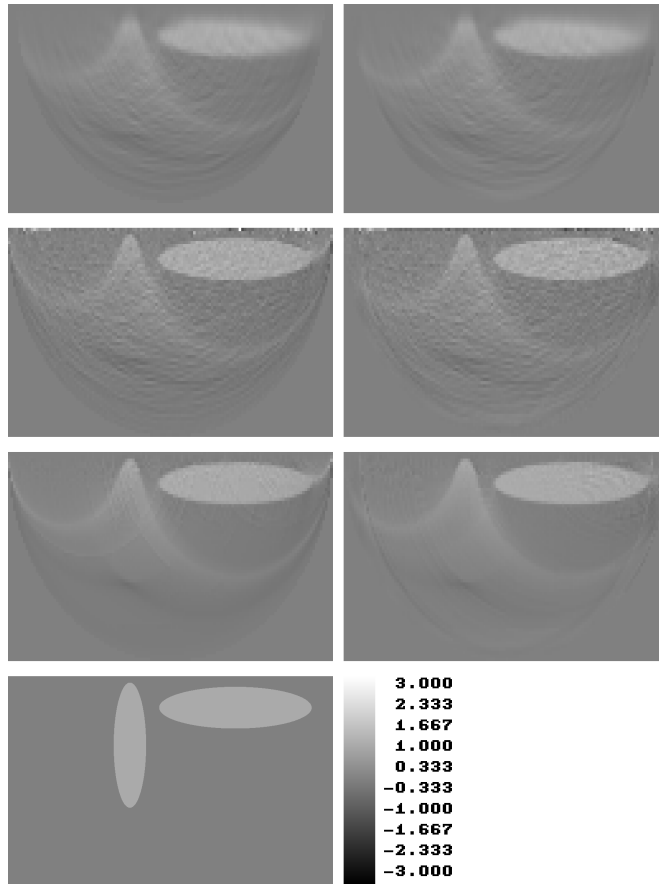


Fig. 11. Reconstruction with the interpolated (right) and given (left) data for noisy data by algorithms: 3.1, 3.2, 4.1—the region is divided into 18 squares (from the top) for exact (left) and noisy (right) data.

apply linear interpolation used nodes (39) as well as (2). To avoid new vertical artifacts we need some filtration. For instance, we set  $R_{j,l} = 0$ , if  $\max(x_k, x_i) > 25$  (i. e. the arc is “almost vertical”).

There is small difference in results for the algorithm 2.1.

On the figures 6 the results of the numerical tests for modified algorithms 3.1, 3.2, and 4.1 are presented.

One can see that some artifacts disappeared or diminished. On the other hand some new artifacts appeared. Note, however, that all the new artifacts that appear, locate

near the boundary  $\{|x| = 1\}$ , in the region of the worst reconstruction.

Reconstruction with interpolated noisy data (Fig. 11) is as stable as reconstruction with noisy data without interpolation. So, data completion procedure seems to be stable.

## 6. Conclusion and future work

We proposed and numerically tested some algorithms for reconstruction of a function from incomplete data of arc means in the seismic tomography model. Algorithms are based on different reductions of the problem to the standard computer tomography reconstruction. The data completion procedure is proposed as well.

Due to strong ill-posedness, reconstruction results unavoidably differ from the original and have artifacts. However, they are still useful. And the question of stability of reconstruction is very important. Our simulation shows that proposed algorithms are quite stable.

Algorithms need further investigation. Specifically, it's desirable to obtain error estimates. These questions will be studied elsewhere.

## 7. Acknowledgement

Preliminary version of the work was presented at the seminar on multimedia and computer graphics at the University of Warmia and Mazury in Olsztyn. The author is grateful to professors Mokrzycki, Mąka and Tatol for their significant remarks.

## References

### 1970

- [1] Lavrent'ev M., Romanov V., and Vasiliev V. Multidimensional inverse problems for differential equations. *Lecture Notes in Mathematics*, 167.
- [2] Harger R. O. *Synthetic Aperture Radar Systems*. Academic Press, New-York.

### 1974

- [3] Shepp L. A. and Logan B. F. The fourier reconstruction of a head section. *IEEE Trans. Nucl. Sci.*, NS-21:21–43.
- [4] Romanov V. G. *Integral Geometry and Inverse Problems for Hyperbolic Equations*. Springer, Berlin.

### 1980

- [5] Herman G. T. *Image Reconstruction from Projections. The Fundamentals of Computerized Tomography*. Academic Press, New-York.

### 1985

- [6] Fawcett J. A. Inversion of n-dimensional spherical averages. *SIAM J. Appl. Math.*, 45:336–341, 1985.
- 1987**
- [7] Tarantola A. Inversion of travel times and seismic waveforms. In G. Nolet, editor, *Seismic Tomography*, pages 135–157. Reidel.
- [8] Hellsten H. and Andersson L. E. An inverse method for the processing of synthetic aperture radar data. *Inverse Problems*, 3:111–124.
- [9] Firbas P. Tomography from seismic profiles. In G. Nolet, editor, *Seismic Tomography*, pages 189–202. Reidel.
- 1988**
- [10] Denisjuk A. and Palamodov V. Inversion de la transformation de radon d’après des données incomplètes. *C. R. Acad. Sci. Paris*, 307, Série I:181–183.
- 1990**
- [11] Alekseev A. S., Lavrent’ev M. M., Romanov M. E., and Romanov V. G. *Theoretical and computational aspects of seismic tomography*, volume 11, pages 395–409. Kluwer Academic Publishers, Novosibirsk.
- 1991**
- [12] Palamodov V. P. Inversion formulas for the three-dimensional ray transform. *Lecture Notes in Math*, 1499:53–62.
- [13] Palamodov V. P. On reliability of reconstruction a velocity field from hodograph. In *Teriya i praktika issledovaniya litosfery*, pages 63–71, Petropavlovsk-Kamchatskii.
- 1999**
- [14] Denisjuk A. Integral geometry on the family of semi-spheres. *Fractional Calculus and Applied Analysis*, 2:42–59.
- 2000**
- [15] Denisjuk A. On reconstruction of a stable part of band-limited function by interpolation. *Proceedings of the Mathematical Institute of Belarus Nat. Acad. Sci.*, 5:60–62.
- [16] Denisjuk A. *On two approaches to the problem of reconstruction from the arc means with incomplete data*, volume 2, pages 11–15. BrSU.
- [17] Palamodov V. P. Reconstruction from limited data of arc means. *Fourier analysis and applications*, 6:25–42.
- 2001**
- [18] Natterer F. *The mathematics of computerized tomography*. SIAM.
- 2008**
- [19] Nolet G. *A Breviary of Seismic Tomography: Imaging the Interior of the Earth and Sun*. Cambridge University Press, New-York.

[20] Kuchment P. and Kunyansky L. Mathematics of thermoacoustic tomography. *Euro. Jnl of Applied Mathematics*, 19:191–224.

**2009**

[21] Agranovsky M, Finch D., and Kuchment P. Range conditions for a spherical mean transform. *Inverse Problems and Imaging*, 3:373–382.